Development of a control-oriented physical model for cylinder pressure peak estimation in SI engines

Development of a Control-Oriented Physical Model for Cylinder Pressure Peak Estimation in SI engines

Vittorio Ravaglioli*, Giacomo Silvagni, Fabrizio Ponti, Nicolò Cavina, Alessandro Brusa
Department of Industrial Engineering – DIN, University of Bologna
* Corresponding author

Matteo De Cesare, Marco Panciroli, Federico Stola
Marelli Europe, Powertrain Division

Abstract

Powertrain electrification is currently considered a promising solution to meet the challenge of CO_2 reduction requested by future emission regulations for the automotive industry. Despite the potential of full electric powertrains, such as Battery Electric Vehicles (BEVs) and Fuel Cell Electric Vehicles (FCEVs), their diffusion has been severely limited by various technological aspects, market drivers and policies. In this scenario, there is a growing interest in Hybrid Electric Vehicles (HEVs) powered by spark-ignited Dedicated Hybrid Engines (DHEs), mainly because of their high efficiency and very-low pollutants. However, since DHEs are usually operated at relatively high loads, with advanced combustions and high in-cylinder pressure and temperature peaks, reliability over time becomes a crucial aspect to be guaranteed by the engine management systems. This work presents development and validation of an innovative control-oriented model, suitable to predict the maximum in-cylinder pressure of SI engines. The procedure is based on information that can be measured or estimated, in real time, on-board a vehicle, and the computational cost is compatible with modern engine control units. To verify accuracy and robustness of the methodology, two different SI engines have been analyzed over their whole operating range: a turbocharged Gasoline Direct Injection (GDI) engine and a Naturally Aspirated (NA) engine. After calibrating the model parameters using both average and cycle-by-cycle data, the accuracy of the maximum in-cylinder pressure estimation has been evaluated always returning errors lower than 3 % between measured and estimated maximum in-cylinder pressure.

1. Introduction

Nowadays, the increase in global temperature, together with the rise of transported people and goods has forced transport legislation boards around the world to establish strict regulation on pollutants and CO_2 emissions. To achieve the Paris Agreement's goals, Greenhouse Gas (GHG) emissions from global road transport need to be dramatically reduced [1, 2]. As a result, decarbonizing the transportation sector is necessary. Following these guidelines, automotive industries developed new technologies and concepts to comply with the "Zero-Emission Challenge" for passenger cars. Several works demonstrate that electrification will play a key role to tackle the problem of CO_2 emissions, starting with the adoption of Hybrid Electric Vehicles (HEVs), called "near-zero Emission Vehicles", and then looking towards the "zero Emission Vehicles", such as BEVs and hydrogen FCEVs [3]. As well known, despite BEVs and FCEVs have the potential to achieve the GHG emissions reduction needed to meet the goals established by the Paris Agreement [1], battery-pack related challenges (energy storage, aging, and weight), lack of charging/filling infrastructure and cost have hindered a wide diffusion of these technologies. However, based on the recent evolution of materials and industrial processes, it is reasonable to expect that these solutions will partially replace internal combustion engines, both in heavy and light-duty vehicles [4], in the long run.

In this scenario, current research is focusing on the development of alternative ICE-based technologies that support GHG reduction in the short/mid-term. Powertrain electrification and the adoption of synthetic fuels and hydrogen will be crucial to improve the overall efficiency and reduce emissions. Typically based on Spark Ignited (SI) engines, modern Hybrid Electric Vehicles (HEVs) combine the benefits of internal combustion engines, such as long driving range, with the high efficiency of electric motors. The improvement in fuel consumption and GHG emission of HEVs is clear and widely documented in the literature. Sens et al. [5] demonstrated the benefits, in terms of CO_2 reduction, provided by HEVs with different configurations, i.e., different locations of the electric motor in the powertrain architecture. Regarding the ICE, Conway et al. [6] quantified the efficiency improvements given by increased compression ratio, optimized turbocharger sizing and reduced enrichment (lean combustion process) of a SI engine coupled with a 48V electric motor. However, to further improve powertrain efficiency, current research has been focused on the so-called Dedicated Hybrid Engines (DHEs), characterized by very high efficiency in a limited operating region and designed to operate with an electric motor, which provides propulsion when the ICE is traditionally inefficient. Several works demonstrated that the Brake Thermal Efficiency (BTE) of DHEs can achieve 45% with a very low CO_2 emission (<20 g/km) [7-9], complying with the HEVs production and homologation requirements. Extreme engine downsizing with high compression ratios [10, 11], Miller-cycle operation [12, 13], very high Exhaust Gas Recirculated (EGR) ratios [14, 15], use of active and passive pre-chamber combustion system [16-18] and advanced combustion approaches such as Gasoline Compression Ignition (GCI) [8, 18-21], Spark Assisted Low-Temperature Combustion (SA-LTC) [22] and compression ignited Low Temperature Combustion (LTC) [23, 24] are the state of art of the technologies used to develop DHE.

Since DHEs are typically based on advanced SI engines with high compression ratio, the mitigation of abnormal combustions (knock and pre-ignition) represents one of the biggest challenges to improve their reliability and controllability. Different approaches have been proposed to reduce the knock tendency, such as Low-Pressure [25, 26] and High-Pressure EGR (LP-EGR and HP-EGR respectively) and Water Injection (WI) [27, 28].

Despite such solutions significantly reduce the probability of abnormal combustions, they also have a strong impact on combustion stability, controllability, and cycle-to-cycle variability. Therefore, running the ICE close to its maximum efficiency (advanced center of combustion, possibly in the maximum brake torque, MBT, condition), might lead to unexpected abnormal combustions, with extremely high maximum pressure peaks, extremely dangerous for the reliability of piston and crank-slider mechanism. As a result, modern DHEs are usually operated with a closed-loop combustion controller, which keeps the center of combustion (CA50) as close as possible to MBT [29, 30]. However, MBT might not always be reached, mainly due to high in-cylinder peak pressure or knocking, which could compromise engine reliability. Therefore, combustion management plays a crucial role in realizing the potential benefits of DHEs (high efficiency and low pollutants).

The most common approaches to realize real-time combustion management achieving both efficiency and reliability goals for DHEs, are based on closed-loop CA50 control. The easiest way to provide combustion feedback (such as, CA50, Pmax, and Knock Index) is through the in-cylinder pressure sensors [31, 32]. When high knock intensities or maximum pressure peaks (coming from a direct measurement) exceed the limits defined by the manufacturer, the controller can dynamically change the CA50 location to meet torque demand while respecting engine reliability limitations. Despite their effectiveness, the high cost and low durability of cylinder pressure sensors make such approaches unsuitable for the needs of large automotive manufacturers. As a result, remote sensing methodologies have been investigated in recent years to replace the combustion feedback coming from the in-cylinder pressure signal. Several works demonstrated that an effective estimation of the combustion feedback can be obtained through a proper processing of signals coming from standard on-board sensors, such as instantaneous crankshaft speed [33, 34], engine block acceleration [35, 36], ion-current sensing [30], and acoustic emissions [37, 38].

Although effective, remote sensing strategies provide indirect feedback on the combustion process and often require physical relationships to correlate combustion-related parameters with sensor output. Due to the complex data processing required to perform such task, the estimation of in-cylinder pressure (and Pmax) is still considered one of the most challenging correlations in remote sensing. Since knock and Pmax are the most important combustion feedback for engine reliability, several authors have developed different methodologies to obtain such information. Zhao et al. [39] demonstrated that both the location of the in-cylinder pressure peak and the maximum pressure rise rate (MPRR) can be effectively obtained by coupling a mathematical model of the reciprocating inertia force excitation with high-frequency processing of vibration velocity signal. Despite remarkable achievements in MPRR estimation, the absolute value of Pmax can not be obtained, making the approach unsuitable for compliance with the more common Pmax limit. Ghamry et al. [40] studied an indirect methodology for in-cylinder pressure measurement using acoustic emission. The authors modeled the entire pressure waveform using two methods: a polynomial fit during the compression stroke, and an autoregressive technique for both the compression and expansion strokes. The integration of these two modeling approaches and the high computational cost of the autoregressive methodology are the main barriers to implementing the model in standard ECUs for real-time applications.

Cruz-Peragon et al. [41] presented a genetic algorithm (GA) based method to determine the instantaneous in-cylinders pressure of internal combustion engines. The authors obtained the pressure trace from two validated GA sub-models that reproduce the engine behavior. The results confirmed the accuracy of the proposed methodology in different engine platforms. However, due to the requirement for a strong understanding of engine behavior (especially because GA models need to be trained and validated), the authors identified end-of-line testing as the main application of the model. In addition to genetic-algorithms, several authors investigated the potential of artificial neural networks (ANNs) for predicting the in-cylinder pressure trace. Among them, Yang et al. [42] designed and calibrated three different ANNs. The aim of their work was to obtain both cyclic Pmax and IMEP prediction using engine related parameters (i.e., injector current, maximum motored pressure and cylinder pressure before the first main injection). Two nonlinear ANNs and an auto-regressive moving average methodology were tested and proved to be promising, but not enough accurate for real-time engine control. In addition, many authors demonstrated the potential of hybrid remote sensing approaches (physical signals processing and machine learning) to improve the accuracy of CA50 estimation. As an example, Pla B. et al [43] highlighted the benefit of coupling a supervised machine learning technique with the information coming from vibrational sensors for better combustion feedback estimation.

Scocozza et al. [44] proposed a data-driven experimental model capable of estimating the Pmax as a function of mainly two parameters, combustion phase and engine load. While demonstrating effectiveness for both cyclic and average Pmax estimation, the large amount of experimental data required to calibrate the model was the main problem for its application to standard engines.

According to the literature, although many efforts have been made to obtain Pmax using different approaches, none of them meets the needs of real-time combustion controllers. To fill this gap, this paper describes a control-oriented physical Pmax model aimed at integrating reliability limitations in existing control strategies for DHEs. After obtaining a simplified formulation of the energy conversion function during a standard spark-ignited combustion process using stock sensors already present in conventional engines and physical relationships, the approach has been validated operating two different engines: 2.0L turbocharged GDI engine, and 1.0L NA engine. The calibration of the simplified energy conversion function for each engine under study has been performed using a small amount of operating conditions representative of the way energy is converted into pressure during the combustion process. Then, Pmax has been estimated over a wide set of experiments, running also EGR and WI, proving its accuracy both considering cycle-by-cycle and averaged values. Thanks to its low computational cost, the proposed model can be readily integrated into a standard ECU and employed as an external reliability limitation (Pmax limit) within the combustion controller. This limit ensures that the minimum achievable CA50, as defined by the engine manufacturer's reliability specifications, is enforced for improved closed-loop control. This implementation utilizes remote CA50 estimation methodologies, allowing for improved closed-loop management without direct combustion feedback. Moreover, the approach can be interesting even if the in-cylinder pressure measurement is available on-board, such as in high performance racing engines or ICE-based stationary power generation, because it might be used to detect measurement drifts over time or sensor failures comparing measured and estimated (through the proposed model) Pmax.

2. Experimental setup

The experimental data used to develop, calibrate, and validate the presented model, were collected running two gasoline SI engines installed in a test cell:

- Engine 1: 4-cylinder 2.0L Turbocharged GDI equipped with LP-EGR and WI.
- Engine 2: 3-cylinder 1.0L Naturally Aspirated with HP-EGR.

The main technical characteristics of the engines under study are summarized in Table 1.

	Engine 1	Engine 2
Engine displacement	1995 cc	999 cc
Number of cylinders	4	3
Bore	84 mm	70
Stroke	90 mm	86.5
Compression ratio	10:1	10.5:1
Valves per cylinder	4	2
Additional systems	LP-EGR + WI	HP-EGR

Table 1. General characteristics of the tested engines.

To monitor the combustion process and calculate the main combustion indexes, such as center of combustion (CA50), Indicated Mean Effective Pressure (IMEP), and Pmax, in-cylinder piezoelectric pressure sensors have been installed in each cylinder of the two engines. The pressure signal has been acquired at 200 kHz and real-time analyzed using AVL IndiCom. To communicate with the Engine Control Units (ECU), an ETAS module coupled with INCA software has been used. This system allowed performing sweeps (starting from the manufacturer calibration values) of the main control parameters which affect the in-cylinder peak pressure (and consequently the knock tendency) such as Spark Advance (SA), throttle position, intake manifold pressure, Lambda (λ), EGR, and WI ratios. Furthermore, to thoroughly investigate each engine operating point, all the engine-mounted sensors have been acquired at lower frequency (100 Hz) using INCA and the engine performance i.e., Brake Mean Effective Pressure (BMEP), torque, and fuel consumption have been logged by the test bench control system. The ECU variable Net Load (NL, defined in Equation 1) has been chosen as engine load index. Such index, defined as the product of the Manifold Air Pressure (MAP) and the volumetric efficiency (η_{int}), represents an estimation of the in-cylinder pressure in correspondence of the intake valve closure, and it is mainly affected by the pressure drop through intake runners and valves and by the displaced volume reduction due to EGR and WI (if present). All the above-mentioned fresh air reductions have been precisely quantified by the manufacturer and included in the volumetric efficiency η_{int}.

$$NL = MAP * \eta_{int} \quad (1)$$

To quantify the exhaust gases recirculated and the amount of water injected (if present) two indexes have been defined and implemented in the ECU by the manufacturer (for η_{int} estimation). Equation 2 defines the water-fuel ratio *r*, where m_f and m_w are the mass of injected fuel and water per cycle respectively. In the same way, Equation 3 defines the EGR ratio EGR_r, where $m_{fresh\ air}$ and m_{EGR} are the mass of fresh air and exhaust gases recirculated in the cylinder per cycle. Furthermore, the real-time availability of *r* and EGR_r allowed proper controlling water and exhaust recirculated gases during the experimental activity, where large variations of these quantities have been performed, the goal being to validate the robustness of the Pmax estimation methodology over a wide range of operating conditions.

$$r = \frac{m_w}{m_f} \quad (2)$$

$$EGR_r = \frac{m_{EGR}}{m_{fresh\ air}} \quad (3)$$

Figure 1 and Figure 2 show the schematic representation of the experimental layout (main sensors and actuators) of the tested engines. As reported in Table 1, Engine 1 is a turbocharged GDI engine equipped with cooled LP-EGR system in which the exhaust gases to be recirculated are extracted after the Three-Way Catalyst (TWC). To control air-fuel ratio and EGR_r, two linear oxygen sensors have been mounted after the turbine and in the intake manifold respectively. Water injection is performed using 4 additional injectors (one per cylinder) placed in the intake runners. Compared to Engine 1, the complexity of Engine 2 (Figure 2) is lower, mainly because boosting and WI systems are not present. Both engines are equipped with standard sensors and actuators mounted on-board the vehicle, such as throttle valve, EGR valve, manifold air temperature and pressure sensor, exhaust temperature sensor.

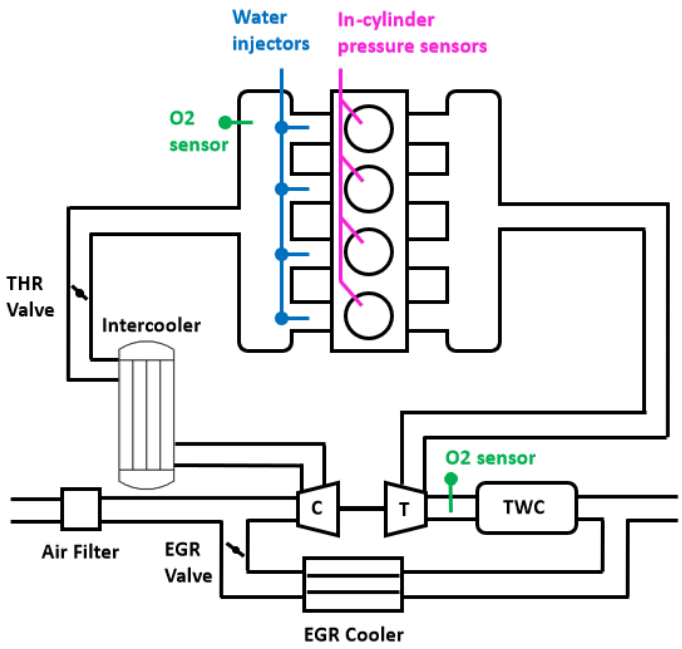

Figure 1. Schematic of the LP-EGR and WI systems of Engine 1

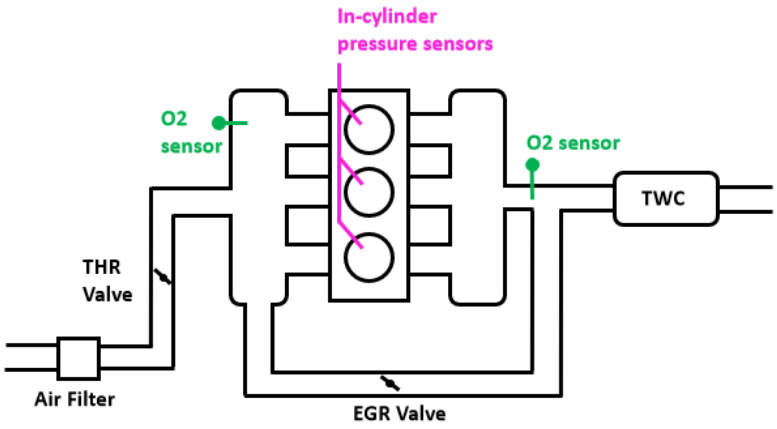

Figure 2. Schematic of the HP-EGR system of Engine 2

To obtain a comprehensive knowledge of the combustion process in the engines considered in this work, both engines have been tested in their whole operating range (defined by the manufacturer). Different combinations of speed, load, and CA50 have been tested as well as different EGR_r and r (if present), and cyclic and average combustion feedback have been measured. The following section will describe the operating conditions during each experimental campaign in detail. By analyzing the experimental data, the Pmax physical model has been formulated using as input signals already present in the standard engine layout. Then, the model has been calibrated using the in-cylinder pressure feedback and then tested in the entire engine operating range.

3. Maximum In-Cylinder Pressure Estimation Model

The most common operating process in modern SI engines for automotive applications is the four-stroke operating cycle, which converts the rise of in-cylinder pressure generated by the combustion into delivered engine torque [45].

The presented methodology for Pmax estimation focuses the attention on the stages in which intake and exhaust valves are closed, i.e., compression and expansion. Given a fixed amount of charge trapped in the cylinder (with a certain temperature), compression and combustion contribute to the achievement of the in-cylinder pressure peak. Although the impact of compression on cylinder pressure can be easily quantified (considering compression as a polytropic process [46]), a simplified model of the interaction between compression and combustion is not straightforward. As a matter of fact, combustion generates a pressure increase (with respect to the motored pressure trace) that strongly depends on the conditions in which the combustion process takes place, i.e., on compression and combustion location within the cycle. To clarify this consideration, the thermodynamic of the simplified (ideal) Seiliger-Sabathé cycle [45] can be analyzed. As it is well known, this cycle schematizes the combustion process as a two-stage heat exchange, one at constant volume and the other at constant pressure.

Referring to the indicated diagram reported in Figure 3, the first stage of the combustion process (2-3, constant volume) follows the compression from 1 (intake valve closure, IVC) to 2. The heat exchange at constant volume (2-3) is the one responsible for the in-cylinder pressure increase, while the following stage (3-3', constant pressure) keeps constant the achieved pressure peak. Once 3' is reached, the expansion process (3'-4) starts, and it ends at the exhaust valve opening (EVO, 4). The compression (1-2) and expansion (3'-4) strokes are considered as isentropic (adiabatic and reversible) transformations. Moreover, the physical properties of the working fluid, such as c_v and c_p, are considered constant throughout the ideal cycle.

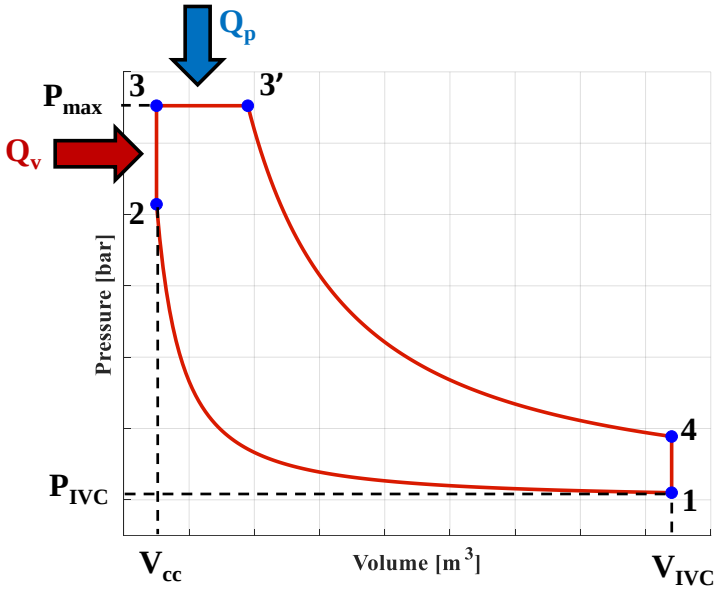

Figure 3. Indicator diagram: ideal engine cycle

Focusing the attention on the combustion process of the simplified engine cycle reported in Figure 3, the total energy introduced (Q_{comb}) can be schematized, through Equation 4, as the sum of two contributions: energy introduced at constant volume (Q_v, from 2 to 3), which generates an instantaneous rise of the in-cylinder pressure when the cylinder volume is equal to the volume of combustion chamber (V_{CC}), and energy introduced at constant pressure (Q_p, from 3 to 3') which keeps the pressure at a constant value while the cylinder volume increases. Since the Seiliger-Sabathé cycle is ideal, the total amount of energy introduced during the combustion process can be considered equal to the energy provided with the injected fuel (100% combustion efficiency), i.e., the product between injected fuel mass (m_f) and lower heating value (LHV) of the fuel. Although real SI engines are characterized by a continuous heat release (no fraction of energy is released at constant volume), the Seiliger-Sabathé cycle was analyzed because it allows highlighting the effect of combustion timing on the impulsivity of the heat release (i.e., the fraction of heat released at constant volume). Moreover, being an ideal cycle, it allows the correlations between the pressure cycle and the control parameters to be made explicit analytically.

$$Q_{comb} = Q_v + Q_p = m_f LHV \qquad (4)$$

As already discussed, the observation of the indicator diagram in Figure 4a clarifies that the pressure increase due to the combustion process is related to $\boldsymbol{Q_v}$, the portion of heat released at constant volume. Such pressure increase starts from the motored pressure peak $\boldsymbol{P_2}$, reached at the end of the compression stroke, that can be easily calculated through Equation 5 (isentropic compression with specific heat ratio $\boldsymbol{\gamma}$).

$$P_2 = P_{IVC} \cdot r_c^{\gamma} \qquad (5)$$

Here, $\boldsymbol{r_c}$ is the compression ratio (which depends on the geometric characteristics of the engine), while $\boldsymbol{P_{IVC}}$ is the cylinder pressure in correspondence of the IVC, where compression starts (that can be easily determined, for a real engine, from mapped volumetric efficiency and direct pressure measurement performed in the intake manifold).

Once the motored pressure peak is determined, to calculate $\boldsymbol{P_{IVC}}$ it is possible to consider that $\boldsymbol{Q_v}$ can be expressed as reported in Equation 6, where $\boldsymbol{T_2}$ and $\boldsymbol{T_3}$ are the cylinder temperature in correspondence of 2 and, 3 respectively and $\boldsymbol{m_{cyl}}$ represent the mass of air trapped in the cylinder.

$$Q_v = m_{cyl} c_v (T_3 - T_2) \qquad (6)$$

As mentioned before, $\boldsymbol{Q_v}$ generates a pressure rise at a constant volume. Thus, $\boldsymbol{T_3}$ can be obtained, applying an isochoric transformation, as reported in Equation 7.

$$T_3 = T_2 \frac{P_3}{P_2} \qquad (7)$$

Substituting Equation 7 into 6 and writing $\boldsymbol{T_2}$ as a function of $\boldsymbol{T_1}$ (isentropic compression), it is possible to highlight the expression of the pressure ratio $\boldsymbol{P_3/P_2}$, yielding (Equation 8):

$$\frac{P_3}{P_2} = 1 + \frac{Q_v}{m_{cyl}\, c_v T_1\, r_c^{\gamma-1}} \qquad (8)$$

Based on the definition of the λ reported in Equation 9, the mass of air can be written as a function of a corresponding fuel mass ($\boldsymbol{m_f}$), simply using Equation 10, where $\boldsymbol{AFR_{st}}$ is the stoichiometric air-to-fuel ratio.

$$\lambda = \frac{AFR}{AFR_{st}} \qquad (9)$$

$$m_{cyl} = m_f \lambda AFR_{st} \qquad (10)$$

In addition, it is possible to define the parameter $\boldsymbol{K_1}$ as the ratio between the amount of energy released at constant volume and the total amount of energy released ($\boldsymbol{Q_{comb}}$). It yields:

$$K_1 = \frac{Q_v}{Q_{comb}} \qquad (11)$$

Equations 4, 10 and 11 can be finally used to rearrange Equation 8 as follows.

$$\frac{P_3}{P_2} = 1 + \frac{K_1 LHV}{\lambda AFR_{st} c_v T_1\, r_c^{\gamma-1}} \qquad (12)$$

As it can be observed in Equation 12, once both engine layout and operating conditions (especially $\boldsymbol{\lambda}$ and $\boldsymbol{T_1}$) are defined, the ratio between pressure peak and motored pressure peak is mainly affected by the fraction of energy released at constant volume ($\boldsymbol{K_1}$). Such behavior can be easily related to combustion speed and location within the cycle. Furthermore, when different characteristics of fuel, mixture preparation, charge motion, and engine geometry are considered, $\boldsymbol{K_1}$ will be affected by different combustion dynamics, potentially resulting in changes to the pressure peak (Pmax). Equation 12 also suggests that, for a given engine operated with a certain fuel, the ratio remains approximately constant at different loads and speeds, while slight variations (with respect to reference air-fuel ratio and intake temperature) can be easily compensated.

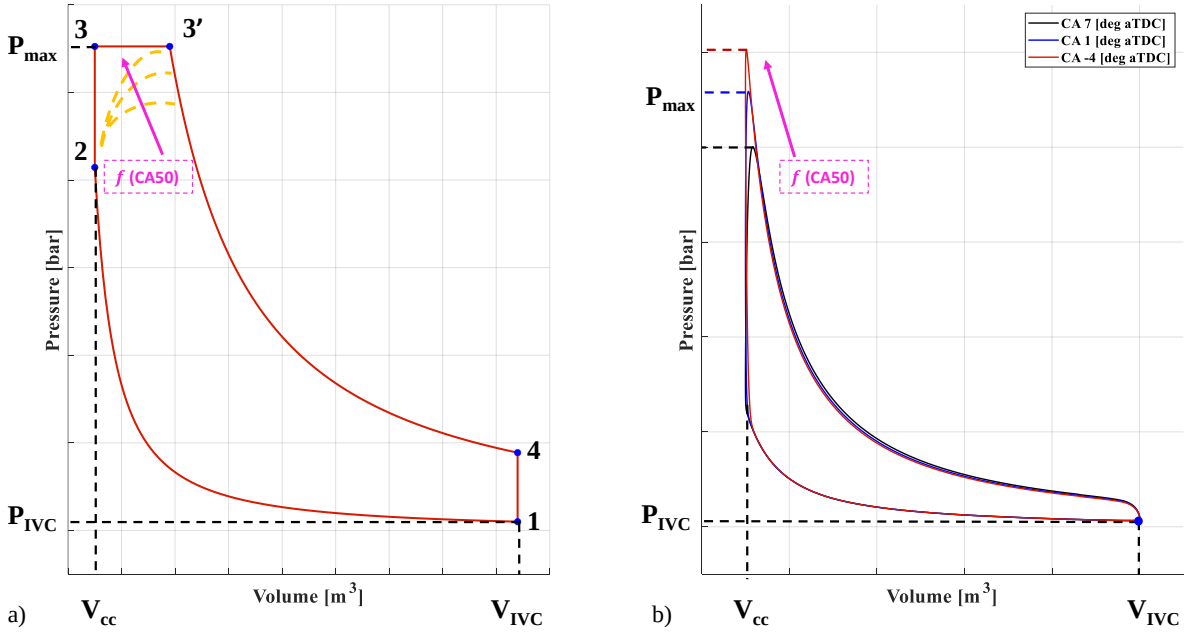

Figure 4. Indicator diagram: a) effect of CA50 on combustion process of the ideal Seiliger-Sabathe cycle, b) effect of CA50 on the real combustion process of the 4-cylinder turbocharged SI engine

Although the above calculations are referred to the indicator diagram of the ideal Seiliger-Sabathé cycle, it is reasonable to expect that similar considerations might be valid also for a real SI engine with some limitations related to the non-idealities of the real energy conversion process. In that case, the fraction of energy released that contributes to the pressure peak rise (corresponding to the key parameter $\boldsymbol{K_1}$) will be strongly dependent on combustion speed, i.e., on the location of the center of combustion (CA50) within the cycle. To better clarify this aspect, Figure 4b shows the comparison between the pressure traces at different values of CA50, obtained running the 4-cylinder turbocharged engine approximately in the same engine operating point (all the engine control parameters were kept constant, except the SA, which was used to vary the CA50). As expected, when the center of combustion of a real cycle is advanced (in the conventional operating range where knock is avoided) $\boldsymbol{Q_v}$ increases because of the higher pressure and temperature in the combustion chamber. As a result, in the same angular range (same volume), a higher portion of the air-fuel mixture releases energy, leading to shorter combustion duration and higher-pressure peak $\boldsymbol{P_3}$.

Due to the differences between real energy conversion (heat and mass losses) and ideal process, described by Equation 12, the fundamental parameter K_1 can not be directly calculated to describe a real energy conversion process for all the engine operating conditions. Therefore, to overcome the limitation of the proposed ideal Pmax model formulation, a control-oriented approach suitable to describe the real energy conversion process as a function of the CA50 will be presented in the following section.

4. Results and Discussion

The above discussed physical considerations, based on the thermodynamic analysis of the Seiliger-Sabathe cycle, could be used to set up a Pmax estimation methodology if the $\boldsymbol{P_3/P_2}$ function reported in Equation 12 is properly identified. Since the proposed approach is based on physical considerations on engines thermodynamic (Seiliger-Sabathé cycle), it is reasonable to consider the Pmax model suitable to describe different SI engine layouts and gasoline-like fuels.

As a matter of fact, the motored pressure peak ($\boldsymbol{P_2}$) can be accurately estimated, starting from the intake pressure at the IVC, approximating the compression stroke as a polytropic process (i.e., through Equation 5 and adjusting $\boldsymbol{\gamma}$ to properly fit the real transformation). To validate the described

$\boldsymbol{P_2}$ estimation methodology and identify γ, while testing the engine in the whole operating range, consecutive misfires were operated (once cylinder at a time was deactivated). As a result, inducing misfire the real motored conditions were generated, and the $\boldsymbol{P_2}$ estimation was validated. Once the motored peak was estimated, it could be multiplied by the identified $\boldsymbol{P_3/P_2}$ function to obtain the estimated peak pressure. For a real engine, the way energy is converted into pressure (quantified by $\boldsymbol{K_1}$) depends on combustion speed and, consequently, on CA50. As a result, it is reasonable to expect that also the $\boldsymbol{P_3/P_2}$ function will depend on CA50. To accurately investigate this dependency and validate the proposed Pmax estimation approach, a large amount of indicated data (especially Pmax and CA50), calculated by the indicating system and acquired running the engines under study over their whole operating range, have been analyzed.

4.1. 4-Cylinder Turbocharged SI Engine

Combustion speed affects the way energy is released (Q_v and Q_p) during the combustion process. Therefore, to investigate the $\boldsymbol{P_3/P_2}$ function, a first experimental campaign has been performed. With the aim of characterizing the impact of CA50 and load on the in-cylinder pressure peak, the engine has been operated at a constant speed of 3000 rpm while both engine load and CA50 have been varied, from low to high load (NL=1, NL=1.5, and NL=2) and CA50 from 7 to 30 deg aTDC respectively. Figure 5 shows the cycle-by-cycle measured Pmax during the CA50 sweeps. Each measured pressure peak has been normalized with respect to the absolute maximum pressure value recorded in the considered sweeps. As expected, retarding the CA50, combustion becomes slower and, consequently, the maximum in-cylinder pressure decreases. During these tests, lambda and the intake temperature were kept approximately constant at 1 and 20 °C respectively.

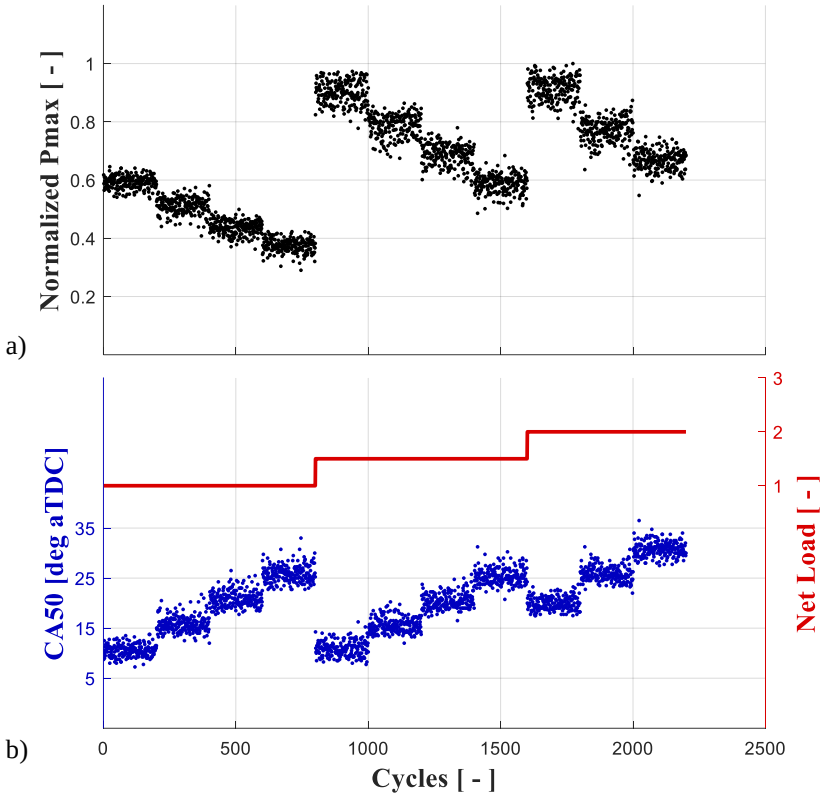

Figure 5. Database for Pmax model calibration at 3000 rpm: a) cycle-by-cycle maximum normalized in-cylinder pressure during CA50 sweeps; cycle-by-cycle Net Load and CA50

To obtain the approximated energy conversion function, the motored pressure peak was determined through Equation 5. For real engines, r_c represents the cylinder volume at IVC (usually different from the bottom dead center) and the volume of the combustion chamber. Regarding γ, for the engine under study it was set to 1.32, suitable to obtain the best fit between measured and estimated motored peak. To determine the P_3/P_2 function, the maximum pressure peak was then divided by the motored pressure peaks, estimated for all the operating conditions of interest. Figure 6 reports the P_3/P_2 ratios, for each cylinder of the engine, as a function of CA50 (in the operating conditions showed in Figure 5).

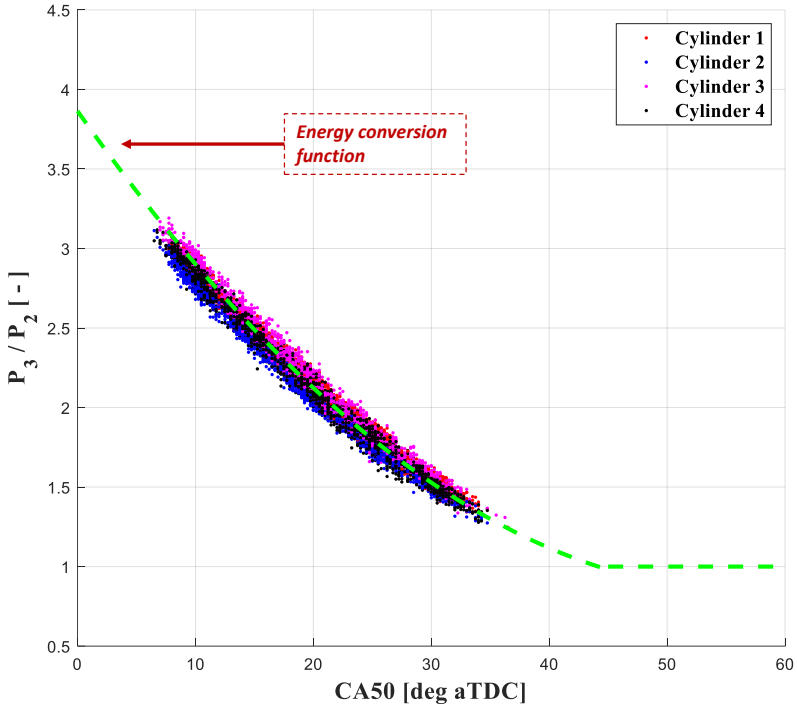

Figure 6. Cycle-by-cycle P_3/P_2 ratio as a function of CA50 for the calibration database and energy conversion function (Pmax physical model) using the 4-Cylinder Turbocharged SI Engine

Figure 6 confirms that, even though different operating conditions are considered (different NL and CA50), when air-fuel ratio and intake temperature are fixed the energy conversion function is unique for the engine under study (and nearly identical for all the 4 cylinders). Figure 6 clearly shows the strong correlation between cyclic P_3/P_2 ratio and CA50 (each dot represents 1 engine cycle characterized by one value of P_3/P_2 ratio and CA50) for each cylinder. As it is evident, P_3/P_2 can be easily described as a quadratic function of the center of combustion. It is important to note that the quadratic function obtained is an approximation of the pressure ratio expressed analytically with Equation 12, and that the change as a function of CA50 quantifies the change in the fraction of energy released at constant volume (expressed by the parameter $\boldsymbol{K_1}$). The simple mathematical formulation (quadratic fitting) and the very low amount of data required to calibrate the model (in principle only one CA50 sweep is needed) makes the proposed approach suitable for industrial applications.

As known from engine theory [33, 34, 47], in the case of delayed combustion the cylinder pressure curve may show 2 peaks in the expansion stroke: the motored pressure peak (due only to charge compression) followed by a second peak due to the heat released during the combustion process. If combustion is very retarded (CA50 values greater than about 44 deg aTDC for the engine under consideration) the second peak (combustion) may be lower than the motored pressure peak. In these cases, the energy conversion function (green dashed line in Figure 6) needs to be bounded at 1. Once the energy conversion function in reference operating conditions (i.e., at reference air-fuel ratio and intake temperature) has been calibrated through a mathematical fitting of the experimental data in Figure 6, the Pmax estimation check can be easily performed multiplying the estimated P_2 (motored pressure peak, determined through Equation 5) by the value of P_3/P_2 at the corresponding *CA50*.

It is important to highlight that the cycle-to-cycle variability that characterizes SI combustion does not affect the accuracy of the proposed estimation methodology, because it is intrinsically considered in the correlation reported in Figure 6. As a matter of fact, the cycle-to-cycle variability is mainly generated by the non-deterministic nature of the combustion process propagation in the combustion chamber. Such aspect causes remarkable differences in terms of energy conversion: a more efficient/advanced combustion produces earlier CA50 and higher Pmax (the opposite occurs for a retarded combustion). Therefore, since the energy conversion dynamic for the engine under study is described by the quadratic function reported in Figure 6, all the engine cycles in each analyzed condition will follow such shape of high cycle-to-cycle variability (as explained before, the engine conditions with CA50 higher than 44 deg aTDC, where the motored pressure is higher than the maximum pressure, are excluded and the P_3/P_2 ratio is always equal to 1). Furthermore, all the four cylinders follow the same trend in terms of energy conversion and slight differences between the P_3/P_2 ratios at same CA50 can be noted.

Once the approximated model has been obtained, to quantify the accuracy of the presented approach the comparison between measured and estimated normalized Pmax (with respect to the maximum in-cylinder pressure value during each sweep) has been performed. Figure 7 summarizes the results of the validation process for cylinder 1, reporting both normalized Pmax values and cycle-by-cycle percent errors, defined in Equation 13.

$$P_{\max\ \_error} = 100 \cdot \frac{(P_{\max\ \_measured} - P_{max\_estimated})}{P_{\max\ \_measured}} \qquad (13)$$

The average absolute percent error of approximately 3% reported in Figure 7 and the calculated Root Mean Squared of the percentage Error (RMSEp) of 1.3% quantify the accuracy of the proposed the Pmax physical model.

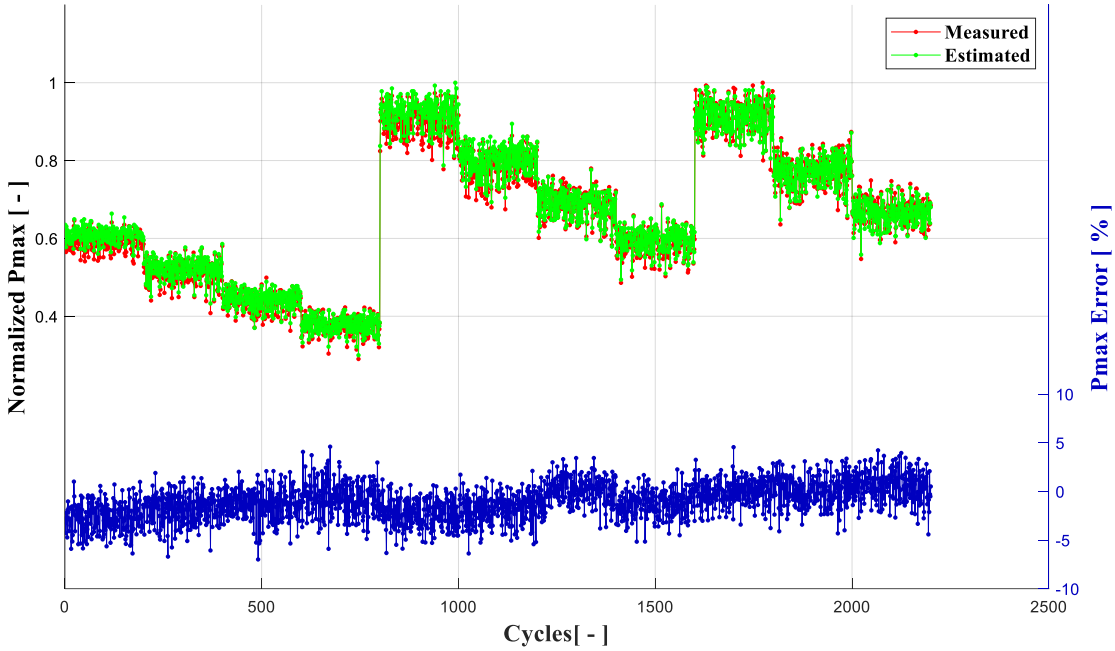

Figure 7. Comparison between cycle-by-cycle measured and estimated normalized Pmax for the calibration database. Model accuracy evaluation of the Pmax estimation: Pmax percentage errors evaluation.

As suggested by Equation 12, the P_3/P_2 ratio (for a certain engine) can be affected by intake temperature and λ. However, once the correlation has been obtained in reference conditions, the effects of the above-mentioned quantities can be easily predicted and compensated. As an example, Figure 8a) shows the impact of different values of λ on the P_3/P_2 ratio in the engine under study (the quadratic function reported in Figure 8 has been obtained through the calibration process shown in Figure 6). Here, the reference condition (i.e., the one at which the function has been mapped) is λ = 1. As expected, the P_3/P_2 ratio becomes lower for leaner values of λ.

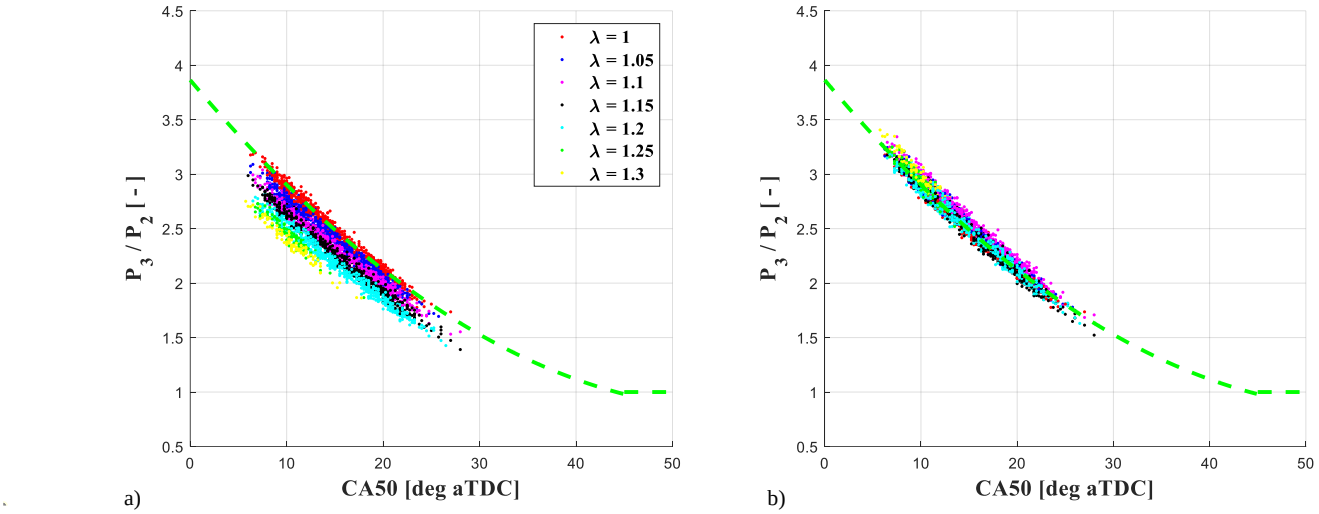

Figure 8. Cycle-by-cycle P_3/P_2 ratio as a function of CA50 changing λ: a) without and with b) lambda compensation at 3000 rpm and different net load using the 4-Cylinder Turbocharged SI Engine

Although the obtained result suggests that a specific $\boldsymbol{P_3/P_2}$ function might be necessary for each value of λ, Figure 8b proves that the effect can be easily compensated using Equation 14. As a matter of fact, the $\boldsymbol{P_3/P_2}$ ratio in different operating condition ($\boldsymbol{\lambda_1}$ and $\boldsymbol{T_1}$), can be determined introducing a correction that depends on the deviation with respect to the reference $\boldsymbol{\lambda_{ref}}$ and $\boldsymbol{T_{1ref}}$ within the general formulation of the energy conversion function in reference conditions ($\boldsymbol{(P_3/P_2)_{ref}}$ described by Equation 12 and simplified by a quadratic function in Figure 6).

$$\frac{P_3}{P_2} = \left[\left(\frac{P_3}{P_2}\right)_{ref} - 1\right] \cdot \frac{T_{1ref}}{T_1} \cdot \frac{\lambda_{ref}}{\lambda_1} + 1 \qquad (14)$$

The flowchart reported in Figure 9 summarizes the procedure for estimating the maximum in-cylinder peak pressure during SI combustion.

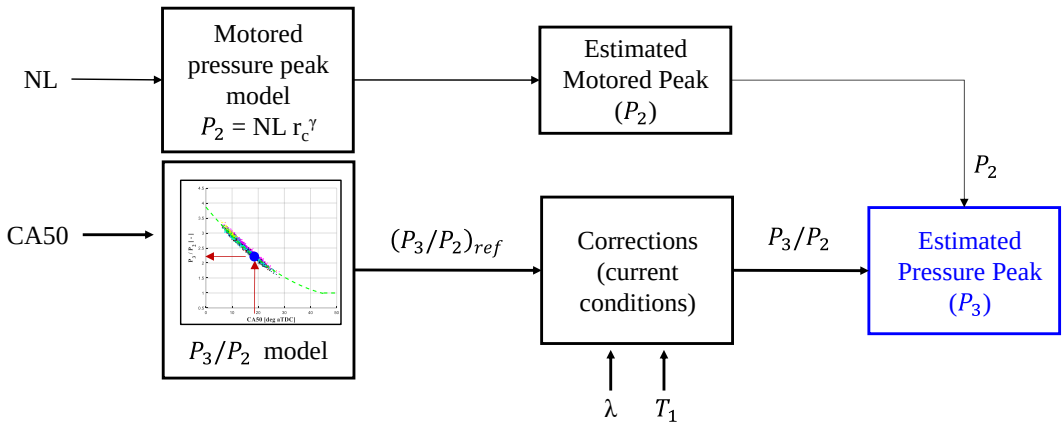

Figure 9. Pmax prediction strategy flowchart based on the developed proposed Pmax model

To check the robustness of the proposed approach, the Pmax model was tested over the whole engine operating range (in terms of load and speed) with its *"Baseline Calibration"*, the one used on-board the vehicles equipped with the engine under study. It is important to mention that, during the experimental activity aimed at investigating the "*Baseline Calibration*", all the engine parameters were kept constant at the values provided by the engine manufacturer (designed for road application in which $\boldsymbol{r}$ and $\boldsymbol{EGR_r}$ were previously defined) in each operating condition. Figure 9 shows the operating conditions investigated during the experimental activity on Engine 1.

Furthermore, to extend the operating conditions far from the engine baseline, the same testing methodology was used to investigate two additional operating modes: *"WI database"* and *"EGR database"*. In the *WI database*, $\boldsymbol{r}$ was varied from 0.2 up to 0.5 (WI was enabled only when NL > 1), while the "*EGR database"* was characterized testing values of $\boldsymbol{EGR_r}$ ranging from 0.02 to 0.18. During the investigation of the two additional operating modes (*"WI database", and "EGR database"*), the experimental data of interest were acquired while performing CA50 sweeps (the area of overlap between the *"WI database"* and "*EGR database"* indicates that both water injection and EGR were used at the same time, while the CA50 was always changed ranging between 8 to 35 deg aTDC in each point). In these cases, only the region of mid-high loads, where the benefit of such methodologies is generally the highest, was explored. Figure 10 summarizes the operating conditions of all the experimental tests used to validate the Pmax model. Since the engine under study typically works with high levels of supercharging, which represent the worst conditions in terms of reliability (the engine might operate close to the Pmax limit), very low loads (*"Excluded Zone"*) were ignored during the Pmax model validation.

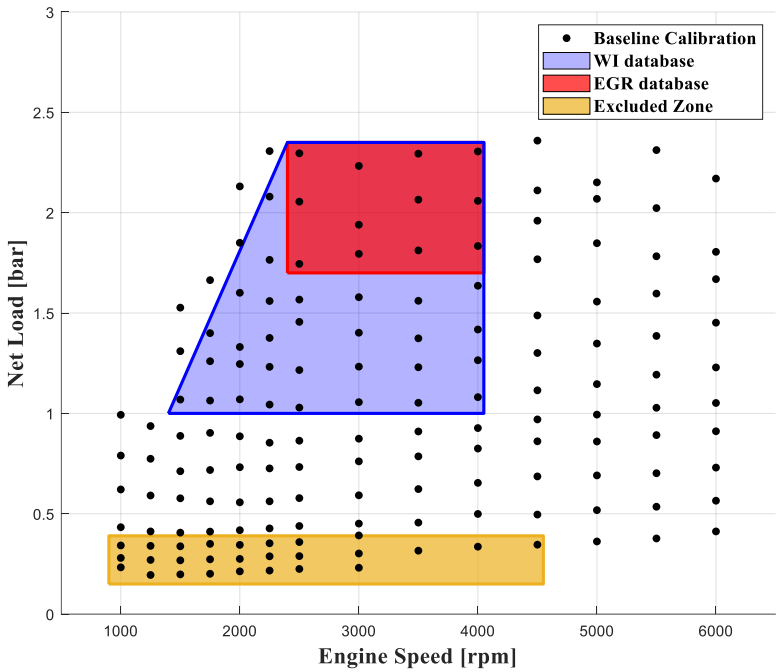

Figure 10. Engine operating conditions used for the Pmax physical model validation for the 4-Cylinder Turbocharged SI Engine

Since the cycle-to-cycle variability does not affect Pmax estimation, the methodology was validated using the average indicating data (in each condition 150 engine cycles were averaged, and Pmax and CA50 were obtained) of each operating point (engine speed and Net Load identify the operating conditions, and additionally *r-*$\boldsymbol{EGR_r}$ if present, while changing CA50) in the above-mentioned databases (*"Baseline Calibration"*, *"WI database"* and *"EGR database*).

Figure 11 reports the P_3/P_2 ratio obtained using the experimental data (averaged data during each operating condition) of the above-described validation databases. The energy conversion function reported in Figure11 (quadratic function) has been obtained through the calibration process shown in Figure 6. Despite considering mean data for each cylinder (represented by the dots in Figure 11), the shape of the energy conversion function does not show significant differences with respect to the reference trend in Figure 6. This means that the identified Pmax model (reported with the green line in Figure 11) can be used to predict the maximum cylinder pressure also in operating points far from the calibration conditions (where r and different values of EGRr with respect to the baseline calibration are used). It is also interesting to notice that, as explained before, operating very retarded CA50 (approximately higher than 44 degCA), the P_3/P_2 function remains approximately constant at 1. This confirms that, due to the high combustion retard, the firing pressure [47, 48] peak remains lower than the motored peak (which is the maximum pressure peak).

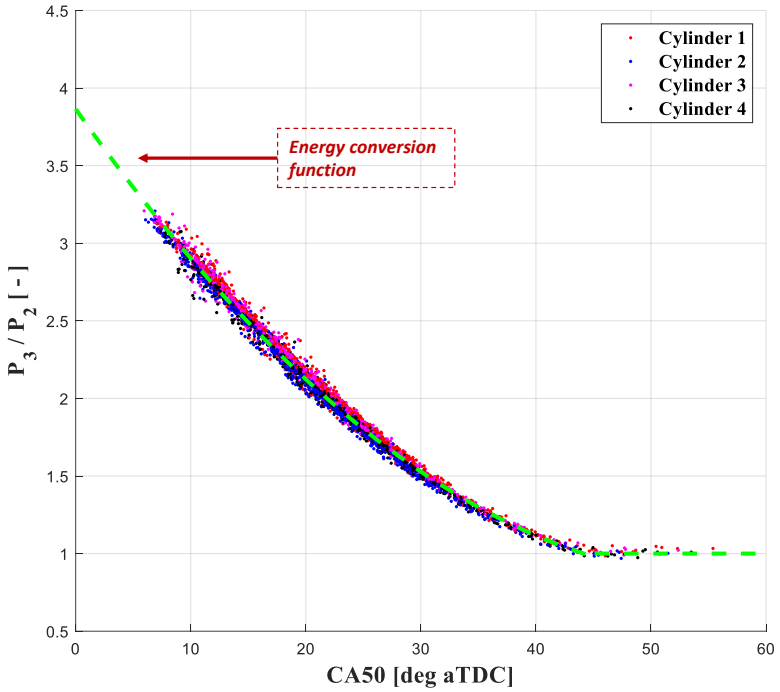

Figure 11. Mean P_3/P_2 ratio as a function of CA50 for the baseline calibration, WI and EGR databases and energy conversion function (Pmax physical model) using the 4-Cylinder Turbocharged SI Engine

Figure 12 shows the comparison between experimental and estimated Pmax in cylinder 1 by using the approximated Pmax model for the three different validation databases previously reported in Figure 10 (mean values are reported). Despite analyzing averaged data from different datasets, the model accuracy does not decrease with respect to the results obtained with the reference calibration data previously shown in Figure 6 (cyclic data were used to calibrate the quadratic function). The results of the *"Baseline Calibration"* database reported in Figure 12a confirm that the model can predict Pmax in operating conditions extremely different from the ones included in the calibration dataset (shown in Figure 6). Moreover, the low value of the percentage errors demonstrates that the energy conversion function is unique, for all the cylinders (Figure 10), over the entire operating range.

As widely discussed in literature, the use of EGR and water injection slows down the combustion process [25, 29]: increasing EGR or water ratio, the combustion will be retarded, and Pmax will decrease consequently. As described before, the strong correlation between P_3/P_2 ratio and CA50 allows to intrinsically consider the impact of different combustion velocities (since CA50 is one of the model parameters) on Pmax. Figure 12b and Figure 12c show the results obtained by applying the Pmax model to operating conditions included in "*EGR database*" and "*WI database*". As already discussed, each operating in Figure 11 corresponds to a CA50 sweep run at fixed value of Net Load and engine speed while changing $\boldsymbol{r}$ *("WI database")* or EGR_r ("*EGR database*") in a range of 0.2 - 0.5 and 0.02 - 0.18 respectively. Based on the above considerations, the analysis of *"EGR database"* and *"WI database"* showed in Figure 12b and Figure 12c respectively, the low percent errors (+/- 5%) and RMSEp (approximately 1.2% and 0.2% respectively) confirm that the performance of the developed model is not significantly affected by these solutions.

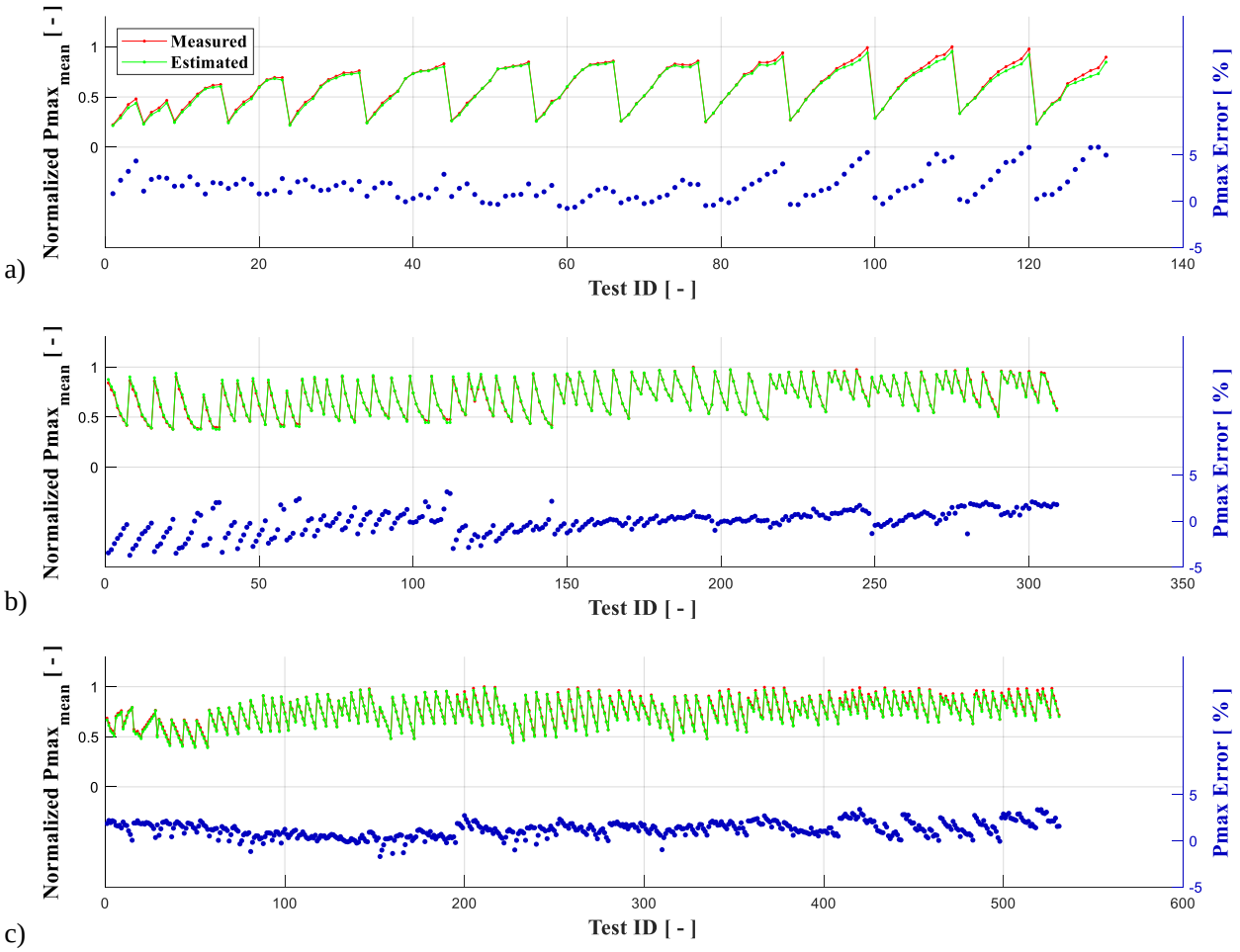

Figure 12. Comparison between mean values of measured and estimated normalized Pmax and model accuracy evaluation (Pmax percentage error) for: a) Baseline calibration database b) EGR database and c) WI database.

It is worth pointing out that Figure 12 shows the Pmax estimation in the cylinder number 1 of the turbocharged SI engine considered in this work using the approximated energy conversion function (Eq. 13) calibrated to describe the real behavior of all the cylinders. To further confirm the model applicability and reliability, Table 2 summarizes the maximum RMSEp in [%], obtained by modelling Pmax with the developed and previously calibrated model on the other three cylinders both in the calibration and validation databases. By looking at the results in Table 2, the low RMSEp values confirm the robustness also in case of different cylinders.

	Cyl 1	Cyl 2	Cyl 3	Cyl 4
CA50 sweep	1.3	0.1	0.3	0.7
Baseline calibration	1.6	0.5	1.3	0.4
WI database	1.1	0.3	1	0.2
EGR database	0.2	1.1	0.3	1

Table 2. Pmax physical model accuracy evaluation in terms of RMSEp using the 4-Cylinder Turbocharged SI Engine: RMSEp, reported in %, comparison for different cylinders and databases.

4.2. 3-Cylinder Naturally Aspirated SI Engine

As showed in the previous section, the proposed Pmax model (Equation 13) can predict the value of the cylinder pressure peak with high accuracy in a spark-ignited supercharged engine. To further extend the validity of the presented approach, it was applied to an engine with different layout and operating range. A wide experimental activity was performed on Engine 2 covering the entire operating range defined by the manufacturer using the standard engine calibration (characterized by $\boldsymbol{EGR_r}$ in the range from 0.02 to 0.15). Following the investigation approach used when the "*Baseline Calibration"* was tested on Engine 1, the Net Load was gradually increased during the experimental activity starting from 1000 rpm. Then, once the maximum load of each operating condition was reached, the engine speed was increased by 500 rpm and the Net Load was varied up to the maximum value defined by the engine manufacture. Figure 13 reports all the operating points (identified by speed and Net Load) in which the engine was tested.

Despite no CA50 sweeps were performed, since Engine 2 is usually operated with HP-EGR using the manufacturer calibration, the obtained database contained enough information to properly calibrate the energy conversion function even operating retarded CA50 (EGR delays the combustion process). In accordance with the analysis of the results obtained from the experimental activities on Engine 1, average data of Pmax and CA50 for each cylinder were considered.

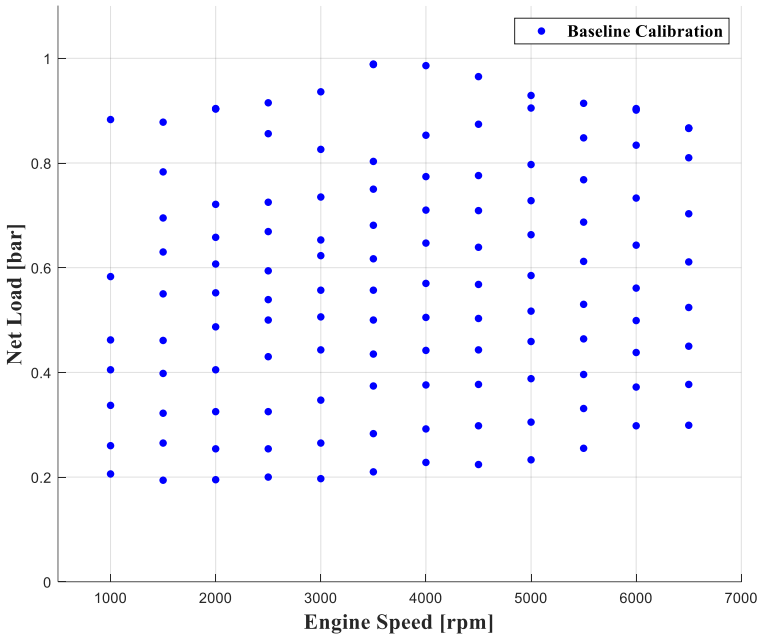

Figure 13. Engine operating conditions used for the Pmax physical model validation for the 3-Cylinder Naturally Aspirated SI Engine

Figure 14 shows the experimental P_3/P_2 ratio as a function of CA50 for the engine operating points reported (averaged data) in Figure 13. As it can be seen, also for Engine 2 the reported experimental points follow unique trend. Therefore, the mathematical formulation proposed in Equation 14 is still applicable as well as the quadratic function. After calibrating the energy conversion function (the model coefficients depend on the engine type), the estimation methodology was applied to the experimental database obtained testing Engine 2, the goal being to assess the performance of the algorithm on the naturally aspirated engine. Figure 15 shows the results obtained for cylinder 1 (averaged data for each analyzed condition).

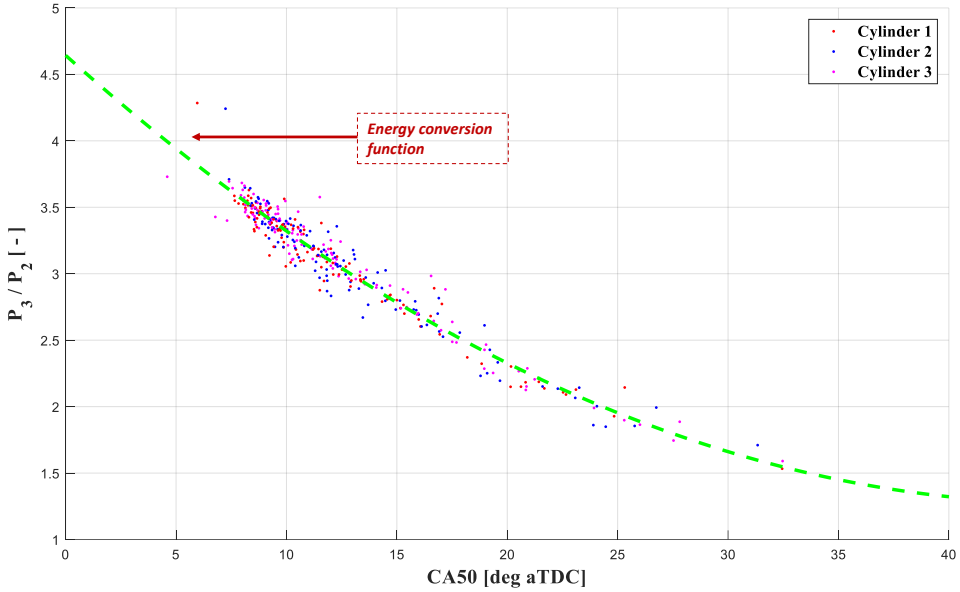

Figure 14. Mean P_3/P_2 ratio as a function of CA50 for the baseline calibration databases and energy conversion function (Pmax physical model) using the 3-Cylinder Naturally Aspirated SI Engine

As it can be observed, the validation procedure returned results similar to the supercharged engine: the comparison between measured and estimated normalized Pmax (with respect to the maximum experimental pressure recorded during the tests) and the evaluation of the Pmax errors (percent error approximately equal to +/-5% and RMSEp around 0.4%) prove that the presented approach is methodological, and can be applied to different SI engines, both supercharged and naturally aspirated, with different layouts and management strategies. Table 3 shows the RMSEp obtained applying the model also to the other 2 cylinders of the engine. As it can be noticed, the low RMSEp values reported in [%] confirm the validity of the model for all the cylinders (also without a time-consuming calibration campaign).

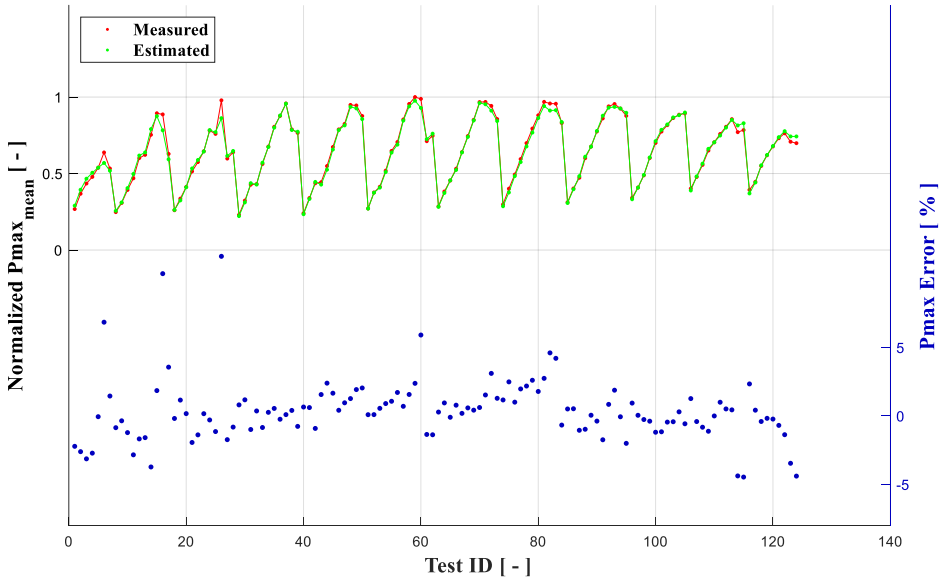

Figure 15. Comparison between mean values of measured and estimated normalized Pmax and model accuracy evaluation (Pmax percentage error) using the 3-Cylinder Naturally Aspirated SI Engine

	Cyl 1	Cyl 2	Cyl 3
Baseline calibration	0.9	0.2	0.4

Table 3. Pmax physical model accuracy evaluation in terms of RMSEp using the 4-Cylinder Turbocharged SI Engine: RMSE, reported in %, comparison for different cylinders

The presented methodology proved to be suitable for the estimation of the in-cylinder pressure peak starting from the estimated cylinder filling (suitable to determine the in-cylinder pressure at the start of the compression process) and the CA50 of each cycle, and the accuracy of the obtained results seems to be compatible with the requirements for engine control. In addition, the computational cost of the algorithm is very low (simple mathematical formulation) and compatible with the real-time operation in a modern ECU. Based on these results, further activity is currently being performed to introduce the algorithm in the combustion control strategies of modern high-efficiency SI engines (especially DHE). In particular, there are multiple ways in which the algorithm can be used on-board. If the engine control knows the value of CA50 (estimated or measured), it can be used to determine the value of the pressure peak (useful, for example, to quantify the load/damage on the engine or, if the engine is equipped with cylinder pressure sensors, to diagnose any malfunction of the sensor itself). Alternatively, the approach discussed in this paper can be used to determine, given a limiting pressure peak value (and thus, given the cylinder filling, the value of the ratio between the limiting peak pressure and the motored peak pressure), the minimum tolerable CA50 value, thereby limiting the spark advance to ensure, under all operating conditions, that reliability limits are met.

5. Summary/Conclusions

This work presents a model-based maximum in-cylinder pressure estimation in SI gasoline engines. To properly investigate Pmax production during the combustion process, two different gasoline SI engines (2.0L GDI and 1.0L NA) have been tested. To study in detail the combustion process, wide experimental activities have been carried out exploring the whole operating range of each engine. By the analysis of the collected data coming from standard and additional sensors, especially the in-cylinder pressure sensors, a strong correlation between Pmax, cylinder filling, intake temperature and center of combustion has been observed, suggesting that these quantities might be used as inputs for a Pmax model.

Based on a thermodynamic analysis of the ideal engine cycle (Seiliger-Sabathe cycle), a physical Pmax model has been developed summarizing the ideal energy conversion function during combustion, which generates the major contribution in terms of maximum in-cylinder pressure production. The analysis of the experimental data confirms what was obtained with the analysis of the ideal cycle (Seiliger-Sabathe). In fact, under the same conditions of inlet temperature and air-fuel ratio, the relationship between the pressure peak and the motored pressure peak is unique and can be approximated with a curve that is a function only of MFB50. In fact, the change in CA50 changes the combustion speed and, consequently, the fraction of fuel burned at constant volume with respect to that burned at constant pressure.

First, the model has been calibrated using a reference set of cycle-to-cycle data, acquired performing a complete *"CA50 sweep"*. Then, the complete Pmax estimation methodology has been applied to different datasets, showing high accuracy both in terms of percentage errors (2.7% for cylinder 1) and RMSEp (1.3% for cylinder 1). In particular, for the first engine under investigation, the approximated model has been used to estimate Pmax in operating conditions significantly different from the ones included in the calibration dataset. Three different databases of averaged data *("Baseline Calibration", "EGR database"* and *"WI database"*), covering the whole engine operating range, have been used. The high accuracy of the approach is confirmed by the obtained results, both in terms of maximum percentage error (3.4% for cylinder 1) and maximum RMSEp (1.6% for cylinder 1). Finally, to further validate the presented approach, the approximated Pmax model has been calibrated and tested using another SI engine (naturally aspirated). The reported results in terms of percentage errors (2.3% for cylinder 1) and RMSEp (0.9% for cylinder 1) confirm robustness, accuracy and general applicability of the proposed Pmax estimation methodology to SI internal combustion engines. The model, developed from analytical considerations applied to an ideal cycle, was calibrated through experimental data and validated over the full operating range of two engines, one supercharged and one naturally aspirated. The approach can thus be used to estimate the maximum in-cylinder pressure during the combustion of SI engines with different number of cylinders and firing orders, operated with high-RON fuels (i.e., gasoline-like fuels), EGR (low and high pressure) and water injection.

As a future step of this work, the presented approximated Pmax model will be used in a real-time engine control unit. In particular, in a combustion phase controller, the discussed approach will be used to determine the center of combustion corresponding to the reliability limits (maxim allowed pressure peak) of high efficiency engines. Since the model has a low computational cost and requires signals already available in a modern standard ECU ($\boldsymbol{P_{man}}$, λ and $\boldsymbol{T_1}$), through its inversion it will be possible to estimate the minimum target CA50 (which corresponds to the maximum energy conversion efficiency) compatible with the reliability limitation of the engine under study. In addition, the Pmax estimation algorithm will be used in a strategy for the automatic diagnostic of in-cylinder pressure sensor malfunctions, which is critical to ensure the reliability of modern high-efficiency engines, managed through the closed-loop control of the measured CA50.

Finally, further activities are currently being performed to generalize the model also considering very lean conditions and different combustion techniques, especially compression ignited engines.

References

1. https://world101.cfr.org/global-era-issues/climate-change/paris-agreement
2. Lalwani, R., Saravanan, N., Veeraputhiran, A., and IlavarasIi, D., "Life Cycle Assessment of a Passenger Vehicle to Analyze the Environmental Impacts Using Cradle to Grave Approach", SAE Technical Paper 2019-28-2581, 2019, https://doi.org/10.4271/2019-28-2581.
3. Joshi, A., "Review of Vehicle Engine Efficiency and Emissions," SAE Technical Paper 2021-01-0575, 2021, https://doi.org/10.4271/2021-01-0575.
4. C. C. Chan, "An overview of electric vehicle technology," in Proceedings of the IEEE, vol. 81, no. 9, pp. 1202-1213, Sept. 1993, https://doi.org/10.1109/5.237530.
5. Sens, M., Pannwitz, M., Forell, A., Brauer, M. et al. "Powertrain Concepts on the Path to CO2 Neutral Mobility," in Presented at the 41st International Vienna Motor Symposium, 2020.
6. Conway, G., Chambon, P., and Alger, T., "Opportunities for Electrified Internal Combustion Engines," SAE Technical Paper 2020-01-0281, 2020. https://doi.org/10.4271/2020-01-0281.
7. Binder, E., Grigoriadis, P., Sens, M., Kitte, J. et al. "A Clean Methane ICE Concept with >45 % Efficiency for Hybrid Powertrains," in Presented at the 29th Aachen Colloquium Sustainable Mobility, 2020.
8. Sellnau, M., Foster, M., Moore, W., Sinnamon, J. et al., "Pathway to 50% Brake Thermal Efficiency Using Gasoline Direct Injection Compression Ignition," SAE Int. J. Adv. & Curr. Prac. in Mobility 1(4):1581-1603, 2019, https://doi.org/10.4271/2019-01-1154.
9. Pan, S., Wang, J., and Huang, Z., "Development of 1.5L Dedicated Hybrid Engine with 42.6% Brake Thermal Efficiency," SAE Technical Paper 2021-01-7031, 2021, https://doi.org/10.427110.4271/2021-01-7031.
10. Darlington, T., Herwick, G., Kahlbaum, D., and Drake, D., "Modeling the Impact of Reducing Vehicle Greenhouse Gas Emissions with High Compression Engines and High-Octane Low Carbon Fuels," SAE Technical Paper 2017-01-0906, 2017, https://doi.org/10.4271/2017-01-0906.
11. Kaminaga, T., Yamaguchi, K., Ratnak, S., Kusaka, J. et al., "A Study on Combustion Characteristics of a High Compression Ratio SI Engine with High Pressure Gasoline Injection," SAE Technical Paper 2019-24-0106, 2019, https://doi.org/10.4271/2019-24-0106.
12. Osborne, R., Downes, T., O'Brien, S., Pendlebury, K. et al., "A Miller Cycle Engine without Compromise - The Magma Concept," SAE Int. J. Engines 10(3):2017, https://doi.org/10.4271/2017-01-0642.
13. Song, S., and Zhang, H., "Performance Study for Miller Cycle Natural Gas Engine Based on GT-Power", Journal of Clean Energy Technologies, Vol. 3, No. 5, September 2015, https://doi.org/10.7763/JOCET.2015.V3.222.
14. Triantopoulos, V., Bohac, S., Martz, J., Lavoie, G. et al., "The Effect of EGR Dilution on the Heat Release Rates in Boosted Spark-Assisted Compression Ignition (SACI) Engines," SAE Int. J. Adv. & Curr. Prac. in Mobility 2(4):2183-2195, 2020, https://doi.org/10.4271/2020-01-1134.
15. Siokos, K., Koli, R., Prucka, R., Schwanke, J. et al., "Assessment of Cooled Low Pressure EGR in a Turbocharged Direct Injection Gasoline Engine," SAE Int J Engines. 8 (2015): 1535-1543, https://doi.org/10.4271/2015-01-1253.
16. Attard, W.P. and Blaxill, H., "A Gasoline Fueled Pre- Chamber Jet Ignition Combustion System at Unthrottled Conditions," SAE Int J Engines. 5 (2012): 315-329, https://doi.org/10.4271/2012-01-0386.
17. Elisa Toulson, E. and Schock, H., J., Attard, W. P., "A Review of Pre-Chamber Initiated Jet Ignition Combustion Systems", SAE Technical Paper, 2010-01-2263, 2010, https://doi.org/10.4271/2010-01-2263.
18. Cooper, A., Harrington, A., Bassett, M., Reader, S. et al., "Application of the Passive MAHLE Jet Ignition System and Synergies with Miller Cycle and Exhaust Gas Recirculation," SAE Technical Paper 2020-01-0283, 2020, https://doi.org/10.4271/2020-01-0283.
19. Ravaglioli, V., Ponti, F., Silvagni, G., Moro, D. et al., "Performance Assessment of Gasoline PPC in a Light-Duty CI Engine," SAE Technical Paper 2022-01-0456, 2022, https://doi.org/10.4271/2022-01-0456.
20. Dempsey, AB, Curran, S, Wagner, R, Cannella, W, & Ickes, A. "Gasoline Compression Ignition (GCI) on a Light-Duty Multi-Cylinder Engine Using a Wide Range of Fuel Reactivities and Heavy Fuel Stratification." Proceedings of the ASME 2020 Internal Combustion Engine Division Fall Technical Conference. ASME 2020 Internal Combustion Engine Division Fall Technical Conference. Virtual, https://doi.org/10.1115/ICEF2020-2929.
21. Cracknell, R., Bastaert, D., Houille, S., Châtelain, J. et al., "Assessing the Efficiency of a New Gasoline Compression Ignition (GCI) Concept," SAE Technical Paper 2020-01-2068, 2020, https://doi.org/10.4271/2020-01-2068
22. Gentz, G., Dernotte, J., Ji, C., and Dec, J. "Spark Assist for CA50 Control and Improved Robustness in a Premixed LTGC Engine Effects of Equivalence Ratio and Intake Boost," SAE Technical Paper 2018-01-1252, 2018, https://doi.org/10.4271/2018-01-1252.
23. M. Krishnamoorthi, R. Malayalamurthi, Zhixia He, Sabariswaran Kandasamy, "A review on low temperature combustion engines: Performance, combustion and emission characteristics", Renewable and Sustainable Energy Reviews, Volume 116, 2019, 109404, https://doi.org/10.1016/j.rser.2019.109404.
24. Kimura, S., Aoki, O., Kitahara, Y., & Aiyoshizawa, E. (2001). Ultra-Clean Combustion Technology Combining a Low-Temperature and Premixed Combustion Concept for Meeting Future Emission Standards. SAE Transactions, 110, 239–246. http://www.jstor.org/stable/44742636.
25. Szybist, James P., Wagnon, Scott W., Splitter, Derek, Pitz, William J., Mehl, Marco," The Reduced Effectiveness of EGR to Mitigate Knock at High Loads in Boosted SI Engines", *SAE International Journal of Engines*, 2017, pp.2305-2318, doi: https://doi.org/10.4271/2017-24-0061.
26. Lenga, H., Hartmann, R., Hyouk Min, B., Grimm, J., Winkler, M., "Low Pressure EGR for Downsized Gasoline Engines, 23rd Aachen Colloquium Automobile and Engine Technology 2014.
27. Iacobacci, Arturo, Marchitto, Luca, Valentino, Gerardo, "Water Injection to Enhance Performance and Emissions of a Turbocharged Gasoline Engine under High Load Condition", *SAE International Journal of Engines*, 2017, pp.928-937, doi: https://doi.org/10.4271/2017-01-0660

28. Cavina, N., Rojo, N., Businaro, A., Brusa, A. et al., "Investigation of Water Injection Effects on Combustion Characteristics of a GDI TC Engine," SAE Int. J. Engines 10(4):2017, doi: https://doi.org/10.4271/2017-24-0052
29. C. Jorques Moreno, O. Stenlåås, P. Tunestål, "Indicated efficiency optimization by in-cycle closed-loop combustion control of diesel engines, Control Engineering Practice, Volume 122, 2022, https://doi.org/10.1016/j.conengprac.2022.105097.
30. Cavina, N., Rojo, N., Businaro, A., & Cevolani, R. (2019)," Comparison between Pressure- and Ion-Current-Based Closed-Loop Combustion Control Performance", SAE International Journal of Engines, 12(2), 219–230. https://www.jstor.org/stable/26840423.
31. Jakob Ängeby, Anders Johnsson, Kristina Hellström, "Knock Detection Using Multiple Indicators and a Classification Approach", IFAC-PapersOnLine, Volume 51, Issue 31, 2018, https://doi.org/10.1016/j.ifacol.2018.10.063.
32. P. Bares, D. Selmanaj, C. Guardiola, C. Onder, "A new knock event definition for knock detection and control optimization", Applied Thermal Engineering, Volume 131, 2018, https://doi.org/10.1016/j.applthermaleng.2017.11.138.
33. Ravaglioli, V., Ponti, F., De Cesare, M., Stola, F., Carra, F., & Corti, E. (2017), "Combustion Indexes for Innovative Combustion Control", SAE International Journal of Engines, 10(5), 2371–2381. https://www.jstor.org/stable/26422620.
34. Ponti, F., Ravaglioli, V., Serra, G., & Stola, F. (2010), "Instantaneous Engine Speed Measurement and Processing for MFB50 Evaluation", SAE International Journal of Engines, 2(2), 235–244. http://www.jstor.org/stable/26275419.
35. Arnone, L., Boni, M., Manelli, S., Chiavola, O. et al., "Block Vibration Measurements for Combustion Diagnosis in Multi-Cylinder Common Rail Diesel Engine," SAE Technical Paper 2009-01-0646, 2009, https://doi.org/10.4271/2009-01-0646.
36. Ponti, F., Ravaglioli, V., Cavina N., and De Cesare M., "Diesel Engine Combustion Sensing Methodology Based on Vibration Analysis." ASME. J. Eng. Gas Turbines Power. November 2014; 136(11): 111503. https://doi.org/10.1115/1.4027363.
37. Barelli L., Bidini G., Buratti C., Mariani R., "Diagnosis of internal combustion engine through vibration and acoustic pressure non-intrusive measurements", Applied Thermal Engineering, Volume 29, Issues 8–9, June 2009, https://doi.org/10.1016/j.applthermaleng.2008.07.025.
38. Cavina, N., Sgatti, S., Cavanna, F., and Bisanti, G., "Combustion Monitoring Based on Engine Acoustic Emission Signal Processing," SAE Technical Paper 2009-01-1024, 2009, https://doi.org/10.4271/2009-01-1024.
39. Xiuliang Z., Yong C., Limei W., Shaobo J., "Real time identification of the internal combustion engine combustion parameters based on the vibration velocity signal", Journal of Sound and Vibration, Volume 390, 2017, https://doi.org/10.1016/j.jsv.2016.11.013 .
40. Ghamry M., Steel J.A., Reuben R.L., Fog T.L.," Indirect measurement of cylinder pressure from diesel engines using acoustic emission", Mechanical Systems and Signal Processing, Volume 19, Issue 4, 2005, https://doi.org/10.1016/j.ymssp.2004.09.004 .
41. Cruz-Peragón F., Jiménez-Espadafor F.," Genetic Algorithm for Determining Cylinder Pressure in Internal Combustion Engines", *Energy & Fuels* **2007** *21* (5), 2600-2607, https://doi.org/10.1021/ef0605495
42. Yang, Z., Steffen, T., Stobart, R., and Winward, E., "A Predictive Model of Pmax and IMEP for Intra-Cycle Control," SAE Technical Paper 2014-01-1344, 2014, https://doi.org/10.4271/2014-01-1344.
43. Pla, B., De la Morena, J., Bares, P., Aramburu, A., "A supervised machine learning technique for combustion diagnosis using a vibration sensor signal", Fuel, Volume 343, 2023, 127869, ISSN 0016-2361, https://doi.org/10.1016/j.fuel.2023.127869 .
44. Scocozza, G., Silvagni, G., Brusa, A., Cavina, N. et al., "Development and Validation of a Virtual Sensor for Estimating the Maximum in-Cylinder Pressure of SI and GCI Engines," SAE Technical Paper 2021-24-0026, 2021, https://doi.org/10.4271/2021-24-0026.
45. Heywood J., Internal Combustion Engine Fundamentals, May 1st, 1988.
46. Huleihil M, Mazor G., "Irreversible Performance Characteristics of Air Standard Otto Cycles with Polytropic Processes", 2012. J Appl Mech Eng 1:111. https://doi.org/10.4172/2168-9873.1000111.
47. Amezcua, E.R., Maldonado, B., Rothamer, D., Kim, K. et al., "Accelerometer-Based Estimation of Combustion Features for Engine Feedback Control of Compression-Ignition Direct-Injection Engines," SAE Technical Paper 2020-01-1147, 2020, https://doi.org/10.4271/2020-01-1147.
48. Hallgren, B. E., & Heywood, J. B. (2003). Effects of Substantial Spark Retard on SI Engine Combustion and Hydrocarbon Emissions. *SAE Transactions*, *112*, 2568–2575. http://www.jstor.org/stable/44742472.

Definitions/Abbreviations

AFR_{st}	Stoichiometric Air-Fuel ratio
BEVs	Battery Electric Vehicles
BMEP	Brake Mean Effective Pressure
BTE	Brake Thermal Efficiency
C_v	Isochoric specific heat
CA50	Mass Fraction Burned 50%
CO_2	Carbon dioxide

DHEs	Dedicated Hybrid Engines
ECU	Engine Control Unit
EGR	Exhaust Gas Recirculation
$\boldsymbol{EGR_r}$	EGR rate
FCEVs	Fuel Cell Electric Vehicles
GCI	Gasoline Compression Ignition
GDI	Gasoline Direct Injection
GHG	Green House Gases
HEVs	Hybrid Electric Vehicles
HP-EGR	High-Pressure Exhaust Gas Recirculation
ICE	Internal Combustion Engine
IMEP	Indicated Mean Effective Pressure
IVC	Instant Valve Closing Angle
$\boldsymbol{K_1}$	Constant volume combustion fraction
$\boldsymbol{LHV}$	Lower Heating Value
LP-EGR	Low-Pressure Exhaust Gas Recirculation
LTC	Low Temperature Combustion
MAP	Manifold Air Pressure
MAPO	Maximum Amplitude Pressure Oscillation
NA	Naturally Aspirated
NL	Net Load
$\boldsymbol{P_{man}}$	Manifold Pressure
$\boldsymbol{P_{max}}$	Maximum in-cylinder Pressure
PRail	Fuel rail pressure
$\boldsymbol{P_2}$	Pressure at TDC

P_3	Pressure after constant volume combustion
Q_{comb}	Total combustion energy
Q_p	Constant pressure combustion energy
Q_v	Constant volume combustion energy
RMSEp	Root Mean Squared of the percentage Error
SA	Spark Advance
SA-LTC	Spark Assisted Low Temperature Combustion
SI	Spark Ignited
THR	Throttle Valve
TWC	Three Way Catalyst
T_1	Manifold Temperature
T_2	Temperature at TDC
T_3	Temperature after constant volume combustion
V_{IVC}	Volume at Intake Valve Close angle
V_{CC}	Combustion Chamber Volume
WI	Water Injection
m_{EGR}	Exhaust gas recirculated mass
m_{cyl}	In-Cylinder trapped mass
m_f	Fuel injected mass
$m_{fresh\ air}$	Fresh air mass
m_w	Water injected mass
r	Water-Fuel ratio
r_c	Geometrical Compression ratio
γ	Specific heat ratio

η_{int}	Intake efficiency
λ	Lambda